International Journal of Hyperthermia

ISSN: 0265-6736 (Print) 1464-5157 (Online) Journal homepage: informahealthcare.com/journals/ihyt20

A thermo-pharmacokinetic model of tissue temperature oscillations during localized heating

C. Chen & R. B. Roemer

To cite this article: C. Chen & R. B. Roemer (2005) A thermo-pharmacokinetic model of tissue temperature oscillations during localized heating, International Journal of Hyperthermia, 21:2, 107-124, DOI: 10.1080/02656730400020769

To link to this article: https://doi.org/10.1080/02656730400020769

Int. J. Hyperthermia, March 2005; 21(2): 107–124

Taylor & Francis
Taylor & Francis Group

A thermo-pharmacokinetic model of tissue temperature oscillations during localized heating

C. CHEN & R. B. ROEMER*

Mechanical Engineering Department, University of Utah, Salt Lake City, UT 84112, USA

(Received 17 May 2004; revised 17 September 2004; accepted 25 October 2004)

Abstract
Thermally-induced large blood flow increases and oscillations have been experimentally observed in both muscle and prostate tissues. However, the bio-physical/-chemical mechanisms underlying these phenomena remain undiscovered. To study the basic nature of these coupled thermal-mass transport processes, this study combines a compartmental vasodilator pharmacokinetics model with a bio-heat-transfer temperature model. The resulting simulated temperature responses to different applied power levels closely match both the overall behaviour and the fine structure of the complex temperature responses observed *in vivo*. This suggests that the coupled thermo-pharmacokinetic model captures the essence of the links between tissue temperature and blood flow oscillations and of the role of the important vaso-active substances. Thus, it appears that such thermo-pharmacokinetic models can provide a basis for helping to understand and quantify the fundamental bio-physical/-chemical processes that couple the transient tissue temperature distributions to blood flow oscillations. Such combined models allow investigators to directly predict tissue blood flow responses to applied power and avoid the need to make *ad hoc* assumptions regulating the blood flow rates present in heated tissues.

Keywords: *Pharmacokinetics, simulations, blood flow, temperature regulation*

Abbreviations: *c, volumetric concentration of the vasodilator, $kg\,m^{-3}$; C_p, specific heat, $J\,kg^{-1}\,K^{-1}$; k, thermal conductivity of tissue, $W\,m^{-1}\,K^{-1}$; P, vasodilator production rate, $kg\,m^{-3}\,s^{-1}$; P_0, baseline vasodilator production rate, $P_0 = \kappa_1 c_{e,0}$, $kg\,m^{-3}\,s^{-1}$; q_{max}, power density on the skin surface, $W\,m^{-3}$; Q, volumetric power density, $W\,m^{-3}$; T, temperature of the endothelium and the smooth muscle (assumed to be equal to the local tissue temperature in this first analysis), °C; T_c, critical temperature at which the vasodilator production rate reaches half of its maximum value, °C; U, vasodilator uptake rate, $kg\,m^{-3}\,s^{-1}$; w, Pennes' equation blood perfusion rate, $kg\,s^{-1}\,m^{-3}$; α_p, attenuation coefficient of planar microwave heating, m^{-1}; β_{BPR}, blood perfusion change coefficient, s^{-1}; β_{PR}, dimensionless amplitude constant for the variation of production rate with temperature such that the production rate plateaus at $P_0(1 + 2\beta_{PR})$ for large temperatures; β_{UR}, vasodilator uptake rate coefficient, s^{-1}; δ, constant which controls how fast the vasodilator production rate increases with temperature, °C; κ_1, vasodilator mass transfer coefficient between endothelium and smooth muscle, s^{-1}; κ_1', vasodilator transfer coefficient between the endothelium and the blood (it is assumed that the vasodilator is swept away rapidly in the blood and, thus, the vasodilator concentration in the blood equals zero*

*Correspondence. Mechanical Engineering Department, University of Utah, Salt Lake City, UT 84112, USA.
E-mail: roemer@mech.utah.edu

ISSN 0265–6736 print/ISSN 1464–5157 online/00/00000107–124
DOI: 10.1080/02656730400020769

and $\kappa_1' = \kappa_1$), s^{-1}; κ_2, vasodilator mass transfer coefficient between smooth muscle and endothelium, s^{-1}; μ, compartmental partition coefficient; ρ, density of the tissue, kg m^{-3}; b, blood; e, endothelial cell; 0, initial/ baseline conditions; s, vascular smooth muscle cell; t, tissue

Introduction

When muscle temperatures increase to high enough values, large, localized blood perfusion increases/oscillations can be induced, resulting in large temperature oscillations [1]. In canine thigh muscle subjected to step changes of microwave heating, four types of responses have been identified:

(1) Type I, at low power levels, temperatures rose monotonically to elevated steady state values;
(2) Type II, at higher powers, when temperatures rose above some 'critical temperature' [2,3], an increase in blood perfusion was activated to give heavily damped temperatures oscillations;
(3) Type III, at even higher powers, temperatures responded as lightly damped or self-sustained large oscillations, with a maximum oscillation of 7°C, and;
(4) Type IV, temperatures rapidly increased above physiologically safe levels at yet higher powers.

Other studies have also observed these types of temperature responses and the associated changes in blood perfusion that occur above a 'critical temperature' in human and animal muscles [2–8] and canine prostate [9–11]. The maximum perfusions measured in the canine prostate using a thermal pulse decay method occurred $\sim$5–7 min after the maximal tissue temperatures were reached [9]. A similar time delay phenomenon was also seen in human experiments that measured both temperature and blood flow using the Xenon clearance technique [3]. In summary, experimental studies have clearly demonstrated the existence of: temperature induced blood flow oscillations in muscle and prostate tissues; four different types of blood flow responses; the existence of a critical temperature phenomena; and a significant time delay between the elevated temperatures and the induced blood flow increases.

Several researchers have attempted to predict and understand these step function induced temperature oscillations. First, Tharp and Zhang [12] employed control theory to successfully simulate all four types of oscillations by using the effective perfusion approach [13] that combines the effects of thermal conduction and blood flow cooling. They assumed that the effective perfusion was a simple polynomial function of the local tissue temperature elevation with a time delay, with three constants that were determined in an *ad hoc* manner. The importance of their study was that it theoretically showed that a time delay between a tissue temperature change and a blood flow rate change was needed to obtain the temperature oscillations observed *in vivo* [3, 4, 11]. However, their time delays of $\tau = 3.4$–30 s were much shorter than those observed experimentally; e.g. $\tau = 5$–7 min in the canine prostate [11]. At approximately the same time, Losev [14] also successfully simulated tissue temperature oscillations by using an effective perfusion term that was assumed to be an integral function of the past temperatures, which implies a time delay between a tissue temperature change and a blood flow change. His study also verified that a time delay can produce temperature oscillations. Again, however, several *ad hoc* coefficients were specified without any bio-physical/-chemical basis. Finally, neither of these two studies provided comparisons between their model predictions and experimental data.

In order to verify and extend the above results, other investigators have successfully reproduced the temperature oscillations in *in vitro* experiments on isolated canine kidneys subjected to ultrasound [15] and water bath heating of pig kidneys [16]. Chen and Xu [16–18] also developed a complete, three-dimensional vascular model of the pig kidney and their point-wise comparisons between model predictions of the temperature oscillations and their *in vitro* experimental data showed good agreement [16, 17]. In these *in vitro* kidney studies [15, 16], the blood perfusion was programmed to linearly increase with temperature with a time delay. None of these investigators explicitly considered the 'critical temperature' phenomenon observed in the previous *in vivo* experiments [2–11]. These studies experimentally verified that (a) the temperature-dependent blood perfusion changes could cause temperature oscillations, and (b) a time delay of ~ 4 min between the initial temperature elevation and the subsequent perfusion increase is needed for temperature oscillations to occur.

In summary, all previous research has been primarily observational or has only attempted to describe the gross characteristics of the temperature and blood perfusion oscillations. No one has yet studied the physiological mechanisms underlying these oscillations, e.g. by providing a physical/chemical basis for the known time delays. However, it is known that there are numerous local factors controlling vessel tone *in vivo* [19], e.g.

(1) Tissue damage and pain reactions result in the release of bradykinin, histamines and prostacyclin, which activate nitric oxide (NO) release, thus dilating blood vessels [19]. The release of bradykinin can also directly dilate blood vessels. As shown by Silva and Antonio [20], the steps responsible for these releases could also be activated by elevated temperatures.
(2) Metabolically-induced localized hypoxia, acidosis or adenosine, K^+ ions, phosphate ion release and hyperosmolarity can each separately induce increased local perfusion [7, 19, 21]. The conditions that create metabolically induced active hyperemia (an increase in the quantity of blood flow to a body part) could possibly be reproduced by high temperatures as proposed by Johnson [21].
(3) It is generally accepted that endothelium-derived nitric oxide (NO) contributes importantly to the local control of blood perfusion under physiological and pathophysiological conditions [22]. In addition, NO production has been linked to increased temperatures [23, 24]. Recently, it has been demonstrated that a nitrite-haemoglobin chemistry linked NO release allows blood vessels to dilate [25, 26], but it is not clear where this NO-release/decomposition reaction occurs [25]. Stamler [26] considered that the vascular storage pool of NO is S-nitrosohemoglobin, while Cosby et al. [25] argued that nitrite rather than S-nitrosothiol is the major pool of NO. The vasodilator NO could be produced by this decomposition process being enhanced in heated tissue.
(4) Based on the earlier work of Kniki et al. [27], there has been a recent suggestion [28] that thermally sensitive Group III and IV aerent fibres could play a role in muscle blood perfusion control. And,
(5) High temperatures could increase the systemic arterial blood pressure, thus causing an increased perfusion [29]. However, during the experiments in Akyurekli et al. [8], blood pressure and pulse were monitored and no significant variations of those parameters were observed. This implies that the change in blood flow during heating could be primarily a localized behaviour.

There is also evidence for the release of neurohumoural agents (e.g. adenosine, histamine, etc.) from local endothelial cells [30] and while thermoreceptors are found abundantly in

skin, evidence for their presence in other anatomical locations is scarce [31]. Taken together, these observations have motivated one to focus the present study on the bio-transport of local, endothelium-produced vaso-active substances. Finally, it should be noted that these heating-induced blood flow oscillations are similar to cold-induced blood flow oscillations—cold-induced vasodilatations (CIVD). However, since the mechanism of CIVD is still debated [32], it is not clear if the mechanisms underlying these two phenomena are related.

The present study extends a simple, generic model [33] to closely reproduce the complex experimental data obtained previously [1, 9]. A thermo-pharmacokinetic model was used to show how the production, diffusion, uptake and storage of key vaso-dilators could introduce the needed time delays. Compartmental modelling used here has been a standard method used to model transport phenomena in the cardiovascular system for a significant time [34] and has been routinely applied in pharmacokinetics [35]. The results show that this simplified thermo-pharmacokinetic model is robust and can help understand the mechanism behind the local tissue temperature oscillations under localized heating conditions.

Formulation

The equations below describe the situation in which a rising endothelial wall temperature increases the rate of production of a vasodilator substance. There are several possible candidates for this substance (e.g. prostacyclin, nitric oxide (NO), adenosine, K^+ ions), but there is currently no consensus on which is the most important [19]. It is also known that such vasodilators can be produced in the endothelium (cardiovascular and peripheral) and then act on the smooth muscles [36]. In any case, each of those substances would be modelled by the same basic pharmacokinetic model, so the approach applied is generic and applicable for any endothelium-produced vasodilators. However, it should be noted that only one of the vasodilators is simulated and any possible combined effect of all vasodilators are not modelled in this study. The chain of events is as follows. First, when the endothelium temperature rises, its rate of production of vasodilator increases. That vasodilator then diffuses into both the blood (where it is swept downstream) and the vascular smooth muscle where it is metabolized and relaxes the smooth muscle, and thus produces an increase in vascular diameter. This in turn increases the local blood flow rate, which in turn decreases the endothelium temperature, thus reducing the production of the vasodilator, which then reduces the level of vasodilator in the smooth muscle, etc., thus potentially producing the observed oscillations. A three-compartment pharmacokinetic model is used to predict the vasodilator concentrations in the endothelium and smooth muscle, with the blood compartment's concentration assumed to be constant. Considering that Pennes bio-heat transfer equation (BHTE) has been extensively used and shown to give practical predictions [37], the BHTE was also applied in this study (i.e. equation (1)). The temporal temperature distribution in the tissue is described by a one-dimensional Pennes bioheat transfer equation [38], with variable tissue cooling elucidated by a spatially and temporally varying blood perfusion rate. The governing equations in the tissue, endothelium and smooth muscle are, respectively:

$$\frac{dT}{dt} = \frac{k}{\rho C_{p,t}} \frac{d^2T}{dx^2} - \frac{C_{p,b}}{\rho C_{p,t}} w(T - T_b) + \frac{Q}{\rho C_{p,t}} \tag{1}$$

$$\frac{dc_e}{dt} = -k_1(c_e - \mu c_s) - k_1' c_e + P \tag{2}$$

$$\frac{dc_s}{dt} = k_2(c_e - \mu c_s) - U \tag{3}$$

All simulations use density, $\rho = 1000\,\mathrm{kg\,m^{-3}}$; specific heat of tissue, $C_{p,t} = 3500\,\mathrm{J\,kg^{-1}\,K^{-1}}$; specific heat of blood, $C_{p,b} = 4186\,\mathrm{J\,kg^{-1}\,K^{-1}}$; thermal conductivity, $k = 0.5\,\mathrm{W\,m^{-1}\,K^{-1}}$; and arterial supplying blood temperature, $T_b = 37^\circ\mathrm{C}$. The tissue's boundary temperatures are kept at $T_1 = 25^\circ\mathrm{C}$ at location $x = 0$ and $T_2 = 37^\circ\mathrm{C}$ at location $x = L$. For the cases that are used to compare with the previous experimental data, the tissue is pre-heated to the initial experimental observed temperatures, 36°C for the canine thigh muscle [1] and 40–41.3°C for the canine prostate [9] and then power is applied at a constant magnitude until the end of the heating. Equations (1–3) are coupled together through the following relations. Considering that endothelium-derived NO is a potent intrinsic vasodilator [39] and the rate of conversion of nitrite to NO exhibits a significant increase at temperatures larger than 40°C [40], the vasodilator production rate, P, is assumed as a hyperbolic tangent function of the local temperature (equation (4)). This shape is similar to the shape of the blood flow vs temperature curves seen experimentally and also includes a threshold temperature effect for perfusion seen in previous studies [2–11],

$$P(T) = \left\{\beta_{\mathrm{PR}}\left\{1 + \tanh\left[\frac{T_c}{\delta}\left(\frac{T}{T_c} - \frac{T_c}{T}\right)\right]\right\} + 1.0\right\}P_0 \tag{4}$$

where the initial production rate is, $P_0 = \kappa_1 c_{e,0}$. β_{PR} is the dimensionless amplitude constant for the variation of production rate with temperature such that the production rate plateaus at $P_0(1 + 2\beta_{\mathrm{PR}})$ for large temperatures. The trend produced by equation (4) is also similar to that for an endothermic transition point for an oxyhaemoglobin solution [41]. The relationship between the normalized production rate, P/P_0, and T is shown in Figure 1.

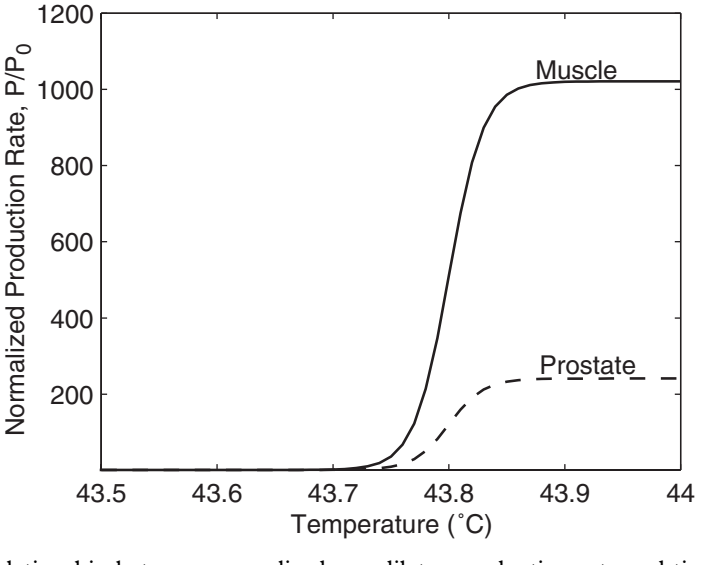

Figure 1. The relationship between normalized vasodilator production rate and tissue temperature.

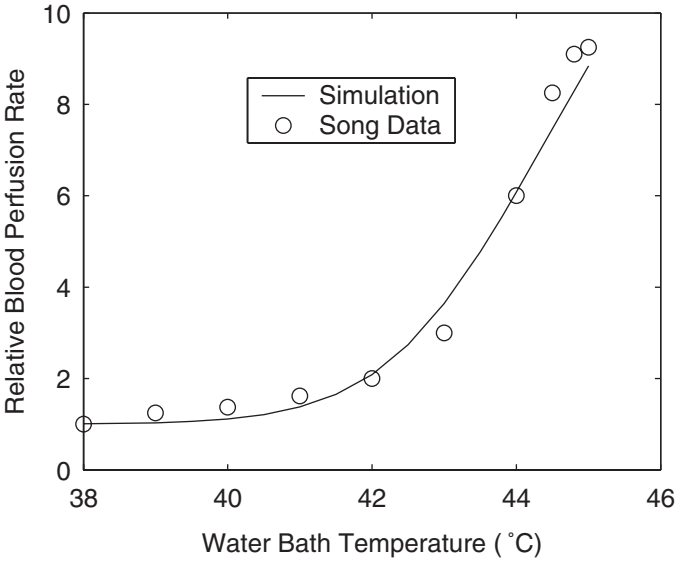

Figure 2. Comparison of the simulated and the measured relationship between blood perfusion rate in the leg muscle of rats and the water bath temperature at the end of 30 min of heating with a constant temperature water bath. The simulation is performed with: $T_c = 43.8^\circ\text{C}$, $\delta = 3.5^\circ\text{C}$, $\beta = 60$.

The uptake rate, U, is assumed to be proportional to the concentration change in the vascular smooth muscle,

$$U = \beta_{\text{UR}}(c_s - c_{s,0}) \tag{5}$$

where β_{UR} is the vasodilator uptake rate coefficient. The blood perfusion, w, is assumed to be proportional to the local concentration of vasodilator,

$$w = w_0 + \beta_{\text{BPR}}(c_s - c_{s,0}), \tag{6}$$

where β_{BPR} is the blood perfusion change coefficient.

In order to verify that the proposed vasodilator production rate model was reasonable, the tissue temperature and blood perfusion rate changes in the leg muscle of rats [7] at the end of 30 min heating with water bath at different constant temperatures were simulated with these thermo-pharmacokinetic models. In the simulation, the diameter of the rat's leg cross-section was assumed to be 0.01 m. The initial tissue temperature and the blood temperature both were set to be 35.5°C based on the information given by Song et al. [7]. Figure 2 shows that the simulation results closely match the experimental data of Song et al. [7]. This indicates that the hyperbolic tangent function adopted in this model is a reasonable correlation to describe the dependence of vasodilator production rate on the tissue temperature. However, in Song et al.'s [7] experiments, the experimental blood perfusion rates were only correlated against the water bath temperature, and not tissue temperatures and, thus, further work was needed to develop appropriate parameter values for the transient temperature oscillation studies. It should be noted that during Song et al.'s experiments, when the water bath temperature was higher than 45°C, blood perfusion rate started to decrease. This turnover phenomenon is not considered in the model since the model assumes that, when temperature rises to $\sim 43.9^\circ\text{C}$, the blood perfusion rate reaches a

plateau and remains at that level for even higher temperatures (see Figure 1). That is, the current paper is not modelling the mechanism of vascular damage that occurs at higher temperature. Therefore, in Figure 2 there is no comparison between this model prediction and Song et al.'s data beyond 45°C.

Given the above equations, attempts were made to closely simulate the two sets of experiments previously performed on canine thigh muscle [1] and prostate [9]. To simulate the canine muscle results, the power deposition of the microwave heating was modelled as an exponential distribution [42], i.e.,

$$Q = q_{\max} e^{-\alpha_p x} \tag{7}$$

where $q_{\max}$ is the power density on the skin surface. The value of α_p was set at $77\,\mathrm{m}^{-1}$ based on the information given by Roemer et al. [1], which also ensures that the specific absorption rate (SAR) at $x = 1.5$ cm depth is close to that determined experimentally (Type IIIB: $83.2\,\mathrm{W\,kg}^{-1}$ when $q_{\max} = 2.64 \times 10^5\,\mathrm{W\,m}^{-3}$ for the simulations and $79.9\,\mathrm{W\,kg}^{-1}$ in the experiment and Type I: $32.5\,\mathrm{W\,kg}^{-1}$ when $q_{\max} = 1.03 \times 10^5\,\mathrm{W\,m}^{-3}$ for the simulations and $34.2\,\mathrm{W\,kg}^{-1}$ in the experiment). This study also used $c_{s,0} = 1.0 \times 10^{-5}\,\mathrm{kg\,m}^{-3}$, $c_{e,0} = 2.0 \times 10^{-5}\,\mathrm{kg\,m}^{-3}$ and $L = 0.15$ m. The critical temperature is set to be $T_c = 43.8$°C and the value of parameter δ is 0.06°C, which represents a steep change in the function value. Since there was no experimental measurement of blood perfusion, its baseline value was estimated as $0.95\,\mathrm{kg\,s}^{-1}\,\mathrm{m}^{-3}$, which is within the baseline range for dogs (0.83–$2.7\,\mathrm{kg\,s}^{-1}\,\mathrm{m}^{-3}$) [43, 44] and also results in the same temperature rise profile (from baseline to first peak) as that observed experimentally. One then iteratively searched the remaining parameter space to determine if one could find a set of parameters that could reproduce the previous *in vivo* experimental results. Such parameters were indeed found and Table I lists the combination of resulting parameter values that best matched the oscillatory experimental temperatures for all four types of temperature responses.

Next, to simulate the experimental canine prostate tissue temperature responses in Xu et al. [9], the same basic model was retained, again with $T_1(x = 0) = 25$°C, $T_2(x = L) = 37$°C, $T_c = 43.8$°C, $\delta = 0.06$°C, $c_{s,0} = 1.0 \times 10^{-5}\,\mathrm{kg\,m}^{-3}$ and $c_{e,0} = 2.0 \times 10^{-5}\,\mathrm{kg\,m}^{-3}$. Based on the measured prostate sizes [9], it was estimated that $L = 0.0178$ m. Since no perfusion rate was given that corresponded to the temperature responses shown in Xu et al. [9], the baseline perfusion rate was chosen to be $w_0 = 2.6\,\mathrm{kg\,s}^{-1}\,\mathrm{m}^{-3}$ based on the fact that the average blood perfusion rate was measured between 2.5–$9.8\,\mathrm{kg\,s}^{-1}\mathrm{m}^{-3}$ in Xu et al. [10]. With $w_0 = 2.6\,\mathrm{kg\,s}^{-1}\,\mathrm{m}^{-3}$, when the value of α_p was set at $110\,\mathrm{m}^{-1}$, the simulation produced the same initial temperature rise rate (from the baseline to the first peak) at the location of $x = 0.01$ m, as observed experimentally [9]. However, no SAR values were given in those *in vivo* prostate studies [9–11] and, thus, $x = 0.01$ m is only an estimate of the location at which the temperature responses were measured. Table I lists the values that were found through the iterative search procedure that gave the best matches between the experimental and simulated oscillatory temperatures.

Table I. Optimized parameter values used to simulate the canine muscle and prostate experiments at all power levels.

Tissue	β_{PR}	β_{UR} (s^{-1})	β_{BPR} (s^{-1})	κ_1 (s^{-1})	κ_2 (s^{-1})	μ
Muscle	510	1.20×10^{-3}	1.80×10^5	5.58×10^{-4}	1.40×10^{-4}	2.0
Prostate	120	5.50×10^{-3}	1.00×10^5	7.92×10^{-4}	1.98×10^{-4}	2.0

Results

Using the values in Table I, four power deposition levels were simulated for the canine thigh experiments. Figure 3 depicts the resulting temperature responses at 1.5 cm into the tissue. It is noticed that Type IIIA and IIIB responses belong to the Type III response that was previously defined. The corresponding local vasodilator concentrations, blood perfusion rates and temperatures are shown in Figure 4(*a*) and the corresponding vasodilator production and uptake rates are shown in Figure 4(*b*) for the Type IIIB response. The comparison between the simulated and experimental results is shown in Figure 5 for the lowest and highest powers (with $q_{\max} = 1.03 \times 10$ [5] $\mathrm{W\,m^{-3}}$ and $q_{\max} = 2.64 \times 10^5\,\mathrm{W\,m^{-3}}$, respectively), which are the Type I and Type III responses. The temporal changes of different terms in the energy balance equation for the Type IIIB response are shown in Figure 6. Simultaneous temperature variation patterns at four tissue depths are shown in Figure 7 for the Type IIIB response. Figure 8 depicts the temperature distributions at 250 min after the initiation of heating for the Type I and Type IIIB responses, plus the predicted temperatures for the same two power levels, but with the perfusion rate remaining at its baseline value. The temperature response curve of Type I overlaps that of the same power level with the fixed constant perfusion rate. Figure 9 shows the simulated temperature responses that best match the experimental prostate data [9].

Finally, a sensitivity study was performed to evaluate the effect of changes in the model's parameter values on the temperature response based on the Type IIIB response for the canine muscle data. The percentage changes in the temperature at the peak of each oscillation, the temperature drop during each oscillation and the peak-to-peak oscillation periods were determined for $\pm 10\%$ changes in the parameters, β_{PR}, δ, β_{UR}, β_{BPR}, w_0, κ_1, and μ.

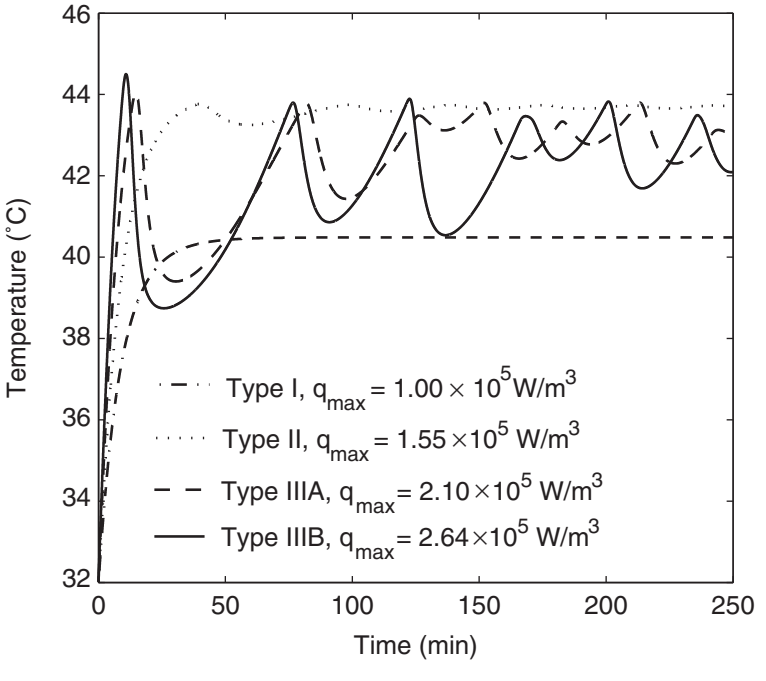

Figure 3. Temperature responses to different applied powers for canine thigh muscle at $x = 1.5$ cm.

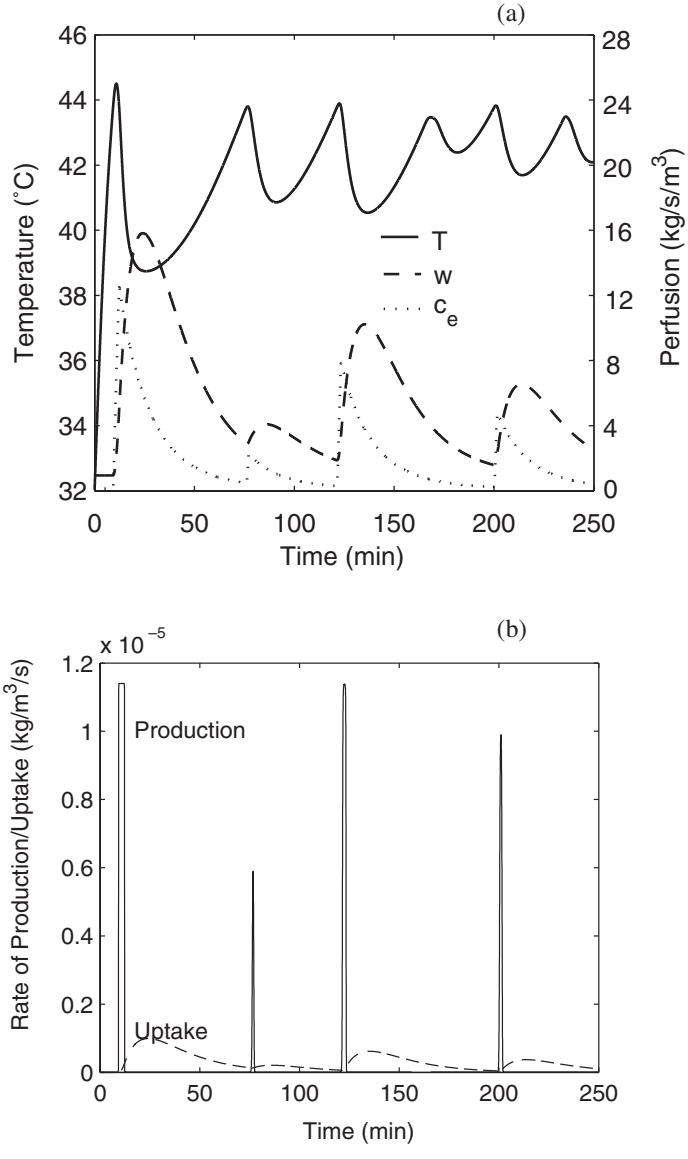

Figure 4. (*a*) Temperature, blood perfusion and endothelial vasodilator concentration for Type IIIB responses of canine thigh muscle. In this figure, c_e **varies** from a minimum of $2\times10^{-5}\,\mathrm{kg\,m^{-3}}$ to a maximum of $1.85\times10^{-3}\,\mathrm{kg\,m^{-3}}$. (*b*) Vasodilator production rate and uptake rate for Type IIIB responses for canine thigh muscle. The uptake rate is magnified by 10 times.

In addition, since small changes in the critical temperature, T_c, could result in large changes in the temperature oscillation pattern, $\pm 3\%$ changes in T_c were used.

Discussion

First, the most significant result from this study is that the simulated temperatures match very well both the overall behaviour and the fine structure of the *in vivo* experimental data

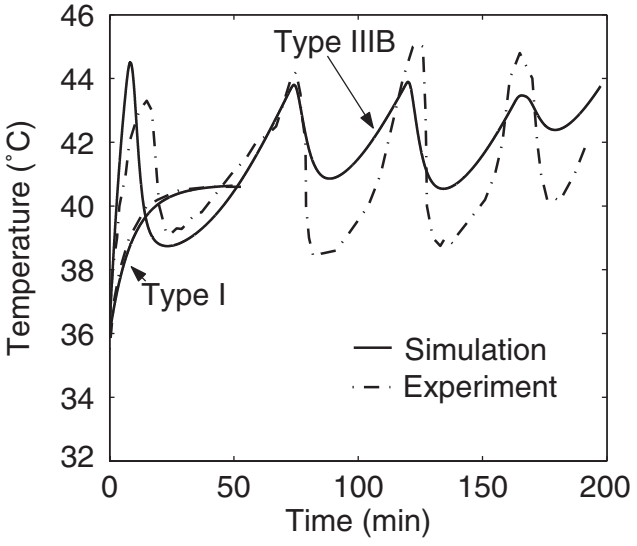

Figure 5. Comparison of simulations and experimental canine thigh results (1) at $x = 1.5$ cm. The SAR values are: Type I: simulation: 32.5 W kg^{-1} and experiment: 34.2 W kg^{-1}; Type IIIB: simulation: 83.2 W kg^{-1} and experiment: 79.9 W kg^{-1}.

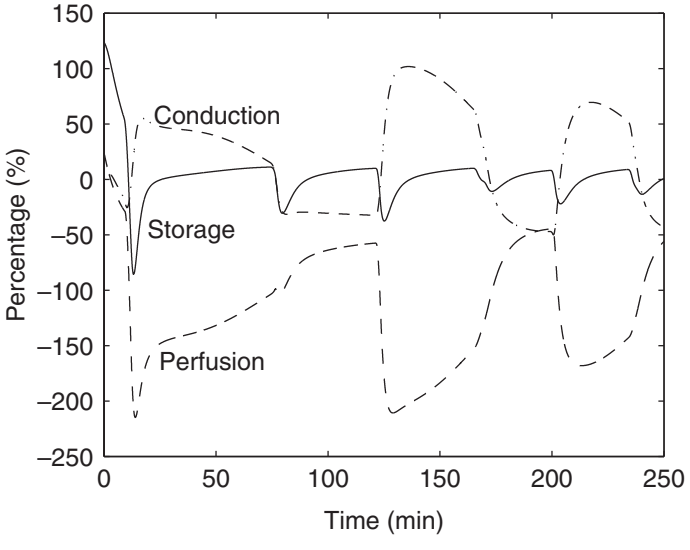

Figure 6. Temporal changes at a depth of 1.5 cm of different terms in the energy balance equation of Type IIIB response relative to the power deposition term.

for both canine thigh muscle (Figure 5) and canine prostate tissue (Figure 8). In terms of overall agreement for the canine muscle, using only one set of tissue parameters the model reproduces the dramatic changes in the patterns of the temperature responses that occur when the applied power magnitude changes (Type I–III responses). More particularly, the simulated temperature profiles are close to the experimental values with nearly the same peak temperatures and oscillation periods and comparable temperature drop magnitudes, especially for the early times. This overall agreement is strengthened

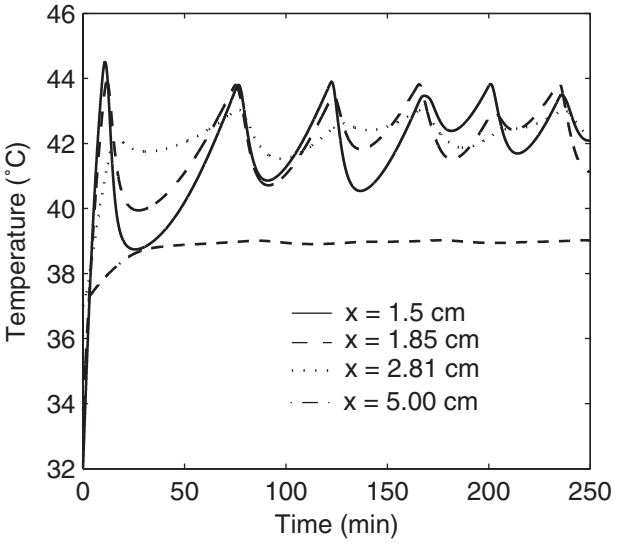

Figure 7. Temperature responses at four different tissue depths when subjected to $q_{max} = 2.64 \times 10^5\,W\,m^{-3}$, Type IIIB of canine thigh muscle.

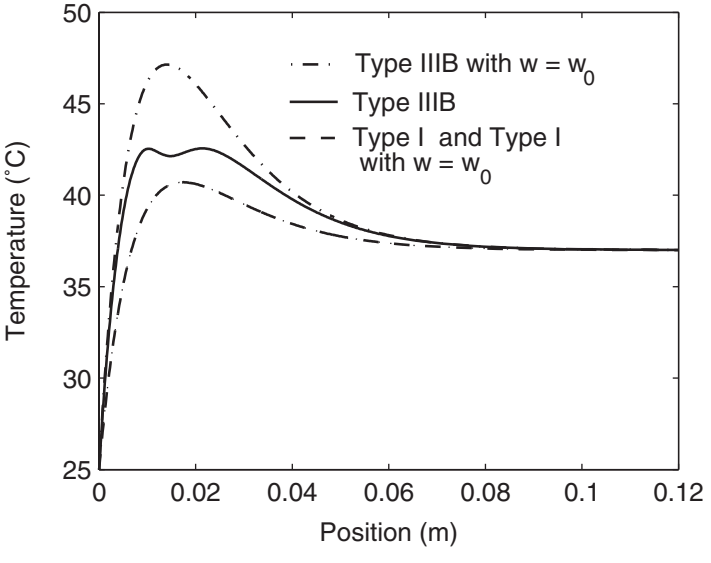

Figure 8. Simulated temperature distributions at the end of 250 min heating for Type I, Type IIIB, and the corresponding cases with constant perfusion rate. Canine thigh muscle.

further by the agreement between the effective perfusions (defined in Roemer [13]) in the simulations (maximum value of 13.1 $kg\,m^{-3}\,s^{-1}$ for the Type IIIB temperature oscillations) and those in the experiments (maximum value of 14.3 $kg\,m^{-3}\,s^{-1}$ for the Type IIIB temperature oscillations). The simulation results also demonstrate that within the Type III patterns, the higher the power level, the larger the oscillation magnitude and the longer it takes to reach the steady state, e.g. compare the Type IIIA and IIIB responses in Figure 3. This is also in agreement with the previous *in vivo* observations [1, 9] and the previous

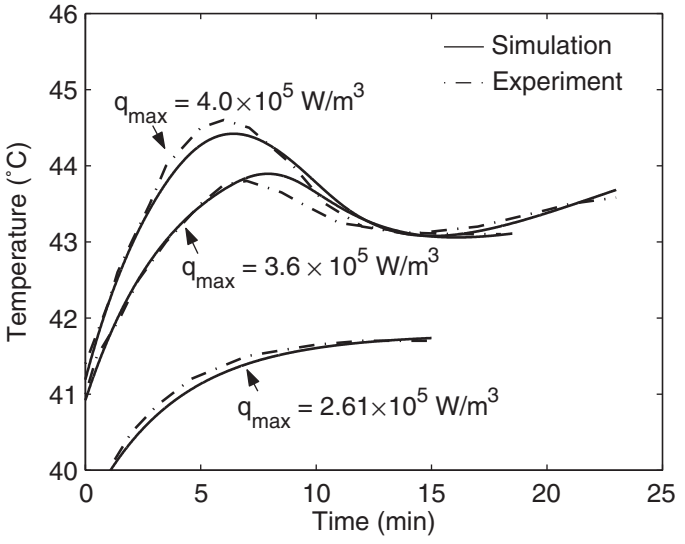

Figure 9. Comparison between the simulation and the experimental canine prostate observations [7].

numerical simulations [14, 16]. Similarly for the prostate, the changes in the experimental temperature response patterns that are induced by varying the applied power are also seen in the simulations and the simulated temperature values agree well with the experimental values. It should be noted that, to date, Type III temperature responses have not been observed in humans. This is probably due to the fact that pain due to high skin temperatures and caution on the part of the clinicians have limited the maximum muscle temperatures attained in humans to date. In the one previous human study which might have produced such results, the heating power was applied for only a short period (~ 30 min) on human thigh muscle [3]. If longer heating had been applied, Type III temperature response might have been observed.

In addition to successfully simulating the major experimental trends observed previously, Figure 5 shows that the following rather complicated, fine structure present in the experimental results is also predicted by the model: (1) the temperature drops very abruptly after it reaches its first peak and then increases much more slowly, with a concave pattern, after it reaches its first minimum; (2) the magnitudes of the temperature drops are much smaller at the later times; (3) the first peak-to-peak period is ~ 67 min and the later periods become successively shorter and shorter. The rapid temperature drops result from the very rapid rate of change of vasodilator production with temperature (Figure 1) when the temperatures are near the critical temperature ($43.8^\circ\text{C} \pm \delta/2$), a dependence that produces the sharp production rate peaks (Figure 4(*b*)). On the other hand, following each temperature minimum, the rate of increase of temperature is smaller than the initial rate of increase of temperature immediately after the power is turned on due to the fact that the blood perfusion is elevated at these temperature minimum points. Those curves are concave since those elevated perfusion values subsequently decrease as the vasodilator uptake decreases the concentration of vasodilator (Figure 4(*a*)). Next, the smaller temperature drops occurring at the later times are caused by localized conduction heating effects from surrounding tissues at higher temperatures (Figure 6). The elevated conduction heating reduces the temperature drops that occur at those maximum blood flow points. Therefore, the later temperature drops are much smaller than the first temperature drop. Finally, these later, smaller

temperature drops require shorter time periods to go through an oscillation cycle, explaining why the first temperature oscillation period is larger than the later temperature oscillation periods. Clearly, the current model can quantitatively account for the fine structure of the experimental results, while such detail has not been predicted by any of the previous models [12, 14, 16]. In particular, Losev's [14] model, which can be shown to be equivalent to adopting a two-compartmental (tissue and blood) model with the vasodilator production rate taking the form of a memory function of the past temperatures, could not reproduce the experimental fine structure. Thus, it appears that the fine structure cannot ever be completely reproduced by simply applying a two-compartmental model.

Secondly, the simulations for canine prostate tissue also capture the same peak temperatures, oscillation magnitudes and periods as observed by Xu et al. [9]. Since the local SAR value was not given in Xu et al. [9], no SAR comparison is possible. The optimal parameter values for the prostate tissue simulations are of the same order of magnitude but different than for the thigh muscle tissue (Table I), i.e. they have different values of β_{PR}, β_{UR}, β_{BPR}, κ_1 and κ_2. This difference could result from differences in the tissue types.

Concerning the spatial distributions of blood perfusion, Akyurekli et al. [8] concluded that regional microwave heating generated a non-uniform blood flow distribution which was a function of the tissue temperature distribution—a result clearly predicted by the current approach. The non-uniform temperature distributions shown in Figures 7 and 8 were also observed in previous *in vivo* experiments [8]. The temperature response patterns at different depths shown in Figure 7 are similar to the temperature response patterns generated by different power levels of heating (Figure 3). This is consistent with the knowledge that the power density varies with tissue depth. Figure 8 also shows the significant cooling effect resulting from the blood perfusion oscillations. The most significant such result is that the oscillatory perfusions flatten and extend the high temperature region. Conversely, when the blood perfusion rate does not change with temperature but is only maintained at its basal level, the tissue temperature rises to much higher values. For the Type I response, the tissue temperature never increases close to the critical temperature, thus a perfusion increase does not occur, making both curves identical.

It has also been observed that, when the power is raised to a high enough level, the tissue temperature will rapidly increase above the physiologically safe level (Type IV temperature response [1]; results not presented here). This happens since the rate of diffusion of the vasodilators from the endothelial cell to the smooth muscle is not fast enough to match the rapid increase in local tissue temperature and, thus, the blood flow does not increase rapidly enough to provide adequate cooling to the local tissue. The dynamics of such time delays are shown in Figure 4(*a*) also. That is, it can be seen that the blood perfusion reaches its peak values ~ 13 min later than the endothelial concentration does. Almost at the same time as the blood perfusion starts to increase, the local tissue temperature reaches its first peak value and then abruptly decreases to its first minimum. At the time that the blood perfusion reaches its peak value, the temperature reaches its minimal value. It can be seen that the vasodilator concentration in the endothelial layer, c_e, starts to increase ~ 12 min after the heating starts. The time delay between the initiation of temperature elevations and the initiation of significant blood perfusion increases also is ~ 12 min. This time delay was determined in an *ad hoc* manner by previous investigators. Here, it is determined through a series of calculations associated with the proposed bio-physical/-chemical processes. In addition, it is interesting to see that there are six over-shoots in the temperature history, but there are only four overshoots in the blood perfusion and concentration change courses. Examining more closely, one can see that for those 'extra' oscillations, the peak temperature is $\sim 43.5^{\circ}$C. At those moments, the rapid increase in vasodilator

Table II. Sensitivity study of canine muscle type IIIB: peak temperatures (PT) results.

Parameter change (±10%)	Variations in peak temperatures (%)			
	1st PT	2nd PT	3rd PT	4th PT
β_{PR}	0	0.1	−0.4	0.7
	0	−0.1	0	−0.7
$T_c(\pm 3\%)$	2.8	3	2.7	3
	−2.7	−3	−3	–
δ	0	0	0	0
	0	0	0	0
β_{UR}	0	0	0	−0.5
	0	0	0	0.5
β_{BPR}	0	−0.1	0	0.5
	0	0.1	−0.2	−0.7
w_0	−0.2	0	−0.2	0
	0.2	0	0	0
κ_1	−0.4	−0.4	0	0
	0.4	0.4	0.5	0.2
μ	−0.1	−0.1	0	0
	0.1	0.1	0.2	0.4

Note: The baseline T_c is at 43.8°C.

production is not triggered. Thus, there is no increase in vasodilator concentration and blood perfusion. The reason that this tissue temperature can reach a peak and then decrease is that conduction cooling from the neighbouring region is so large that it adds to the blood perfusion cooling and overcomes the microwave heating (shown in Figure 6).

The sensitivity study (Table II) shows that the critical temperature (T_c) is the parameter that most significantly determines the peak temperature, with an almost one-to-one correspondence of changes in the maximum temperature with changes in the critical temperature. Changes in all other parameters have little effect on the peak temperatures. From these studies, for canine skeletal muscle, the peak temperatures and the steady state temperatures appear to be close to the critical temperature. In the thermo-pharmacokinetic model developed here, T_c is the critical parameter that determines the speed and magnitude of blood perfusion increases. Indeed, an order of magnitude approximation of steady state conditions for applied powers high enough to induce oscillations using the parameter value of Table I, gives that

$$T_{ss} \approx T_c \tag{8}$$

Although not shown here, the simulation results also show that, for the canine prostate under appropriate high power levels of heating, the steady state local tissue temperature also reaches this value. Interestingly, as in the experiments, this order of magnitude analysis shows that, for high enough values, the applied power has a negligible impact on the steady state temperature reached since increased power levels are directly compensated for by increased blood flow cooling.

The sensitivity study (Table III) also shows that the critical temperature (T_c) plays important roles in determining the magnitude of the first temperature drop. Table IV shows that changes in the uptake rate parameter β_{UR} will induce the largest changes in the first oscillation period (OP) and has strong effects on later OPs and the diffusion

Table III. Sensitivity study of canine muscle type IIIB: magnitude of temperature drop (TD) results.

Parameter change (±10%)	Variations in temperature drop (%)			
	1st TD	2nd TD	3rd TD	4th TD
β_{PR}	1.0	−11.5	−1.0	88.6
	−1.0	11.5	−57.1	−77.1
T_c(±3%)	0	−0.3	−59.4	–
	−16.7	−60.0	−53.1	–
δ	0	0	−1.6	−5.0
	0	0	1.6	5.0
β_{UR}	−1.0	5.7	−10.7	−88.6
	1.0	−7.6	3.6	117.1
β_{BPR}	0.5	−11.4	−1.8	94.1
	−0.8	11.4	−57.1	−77.1
w_0	−5.0	11.4	−66.1	−54.3
	5.0	−11.4	−3.6	82.9
κ_1	−1.0	−15.2	−8.9	77.1
	1.0	15.2	−85.7	−65.7
μ	0.5	−13.3	−3.6	94.3
	−0.8	13.3	−60.7	−71.4

Note: The baseline T_c is at 43.8°C.

Table IV. Sensitivity study of canine muscle type IIIB: temperature oscillation period (OP) results.

Parameter change (±10%)	Variations in temperature oscillation period (%)			
	1st TD	2nd TD	3rd TD	4th TD
β_{PR}	1.0	−5.5	−6.7	19.8
	−1.0	4.1	−43.2	−44.0
T_c(±3%)	0	−4.0	−27.0	−28.1
	−2.0	−24.6	−51.4	–
δ	0	0	0	−2.0
	0	0	0	2.0
β_{UR}	−5.8	−1.3	−16.1	−76.0
	5.8	1.3	2.8	7.9
β_{BPR}	1.0	−5.5	−6.8	19.8
	−1.0	4.1	−43.2	−44.0
w_0	0	6.9	−45.9	−39.9
	0	−6.9	−10.7	−19.8
κ_1	−4.8	−12.3	−14.9	13.9
	4.8	12.3	−63.5	−52.0
μ	0	−5.5	−8.0	20.0
	0	5.5	−45.9	−39.9

Note: The baseline T_c is at 43.8°C.

coefficient κ_1 is the second important parameter that can induce large changes in the OPs. Increases in β_{UR} and κ_1 will shorten the OPs. Increases in β_{UR} increase the vasodilator consumption rate and thus elevated blood flow rates cannot be maintained and the tissue temperature quickly increases from the minimum to the maximum. Increases in κ_1 increases the vasodilator diffusion from the endothelial cell to the smooth muscle which speeds up the blood flow changes. Therefore, the larger β_{UR} and κ_1, the shorter the oscillation period is.

In summary, these results clearly indicate that the proposed thermo-pharmacokinetic mechanism could be responsible for the previously observed experimental temperature oscillations. They also give confidence in the modelling approach—so that such perfusion models can be more confidently used (when expanded to include more realistic details) to optimize and control blood flow rates in specific applications (e.g. high temperature therapy [45], tissue oxygenation in chemoradiotherapy [46] and targeted drug delivery in chemotherapy [47]).

Future studies will aim at developing more accurate models of uptake and production rates, multi-dimensional mass transfer [48] and more accurately determining the parameters needed in the compartmental modelling. For example, the (non-temperature related) pharmacokinetics of the vasodilator NO have been studied and modelled extensively (see Buerk [49]) and future such research could yield the parameters needed in improved thermo-pharmacokinetic models. In addition, the use of more detailed chemical diffusion models, such as for NO [48] could add additional information to the current results. The results from this study provide a basis for understanding how blood flow increases with localized heating, knowledge that can be used to design physiological experiments to identify the key vasoactive agents present during heating. Such knowledge could prove very useful in the optimization and model-based control of all thermal therapies.

Conclusions

Most importantly, this study shows that the simulated temperature responses to different power levels quantitatively match the overall behaviour and fine structure observed in previous *in vivo* experiments. This demonstrates that the newly developed thermo-pharmacokinetic model captures the essence of the links between tissue temperature and blood flow oscillations and the activities of the vasoactive substances. Thus, it appears that such thermo-pharmacokinetic models can provide a fundamental basis for coupling the tissue temperature distributions to blood flow changes, thus providing method for predicting blood flow as a function of temperature.

Acknowledgements

This research was partially supported by NIH (CA R01 - 87785). The authors appreciate the assistance of Dr David Symons regarding possible mechanisms underlying the blood flow oscillations during localized heating and of Dr Steve Kern regarding the pharmacokinetic models.

References

1. Roemer RB, Oleson JR, Cetas TC. Oscillatory temperature response to constant power applied to canine muscle. Am J Physiol 1985;249:153–158.
2. Guy A, Lehmann J, Stonebridge J. Therapeutical applications of electromagnetic power. In: IEEE, 1974;55–75.
3. Sekins K, Lehmann J, Esselman P, Dundore D, Emery A, Delateur B, et al. Local muscle blood flow and temperature responses to 915 MHz diathermy as simultaneously measured and numerically predicted. Arch Phys Med Rehabil 1984;65:1–7.
4. Richardson A, Imig C, Feucht B, Hines H. Relationship between deep tissue temperature and blood flow during electromagnetic irradiation. Arch Phys Med 1950;31:19–25.

5. Lehmann J, Guy A, Delateur B, Stonebridge J, Warren C. Heating patterns produced by short-wave diathermy using helical induction coil applicators. Arch Phys Med 1968;49:193–198.
6. Sekins K, Dundore D, Emery A, Lehmann J, McGrath P, Nelp W. Muscle blood flow changes in response to 915 MHz diathermy with surface cooling as measured by Xe133 clearance. Arch Phys Med Rehabil 1980;61:105–113.
7. Song CW, Lokshina A, Rhee J, Patten M, Levitt SH. Implication of blood flow in hyperthermic treatment of tumors. IEEE Trans Biomed Eng 1984;BME-31:9–16.
8. Akyurekli D, Gerig L, Raaphorst G. Changes in muscle blood flow distribution during hyperthermia. Int J Hyperthermia 1997;13:481–496.
9. Xu LX, Zhu L, Holmes KR. Thermoregulation in the canine prostate during transurethral microwave hyperthermia, part I: temperature response. Int J Hyperthermia 1998;14:29–37.
10. Xu LX, Zhu L, Holmes KR. Thermoregulation in the canine prostate during transurethral microwave hyperthermia, part II: blood flow response. Int J Hyperthermia 1998;14:65–73.
11. Xu LX, Zhu L, Holmes KR. Blood perfusion measurement in the canine prostate during transurethral hyperthermia. Ann NY Acad Sci 1998;858:21–29.
12. Tharp HS, Zhang WW. Analytical study of temperature oscillations in living tissues. IEEE Trans Biomed Eng 1993;40:108–110.
13. Roemer R. The local tissue cooling coefficient: a unified approach to thermal washout and steady state 'perfusion' calculation. Int J Hyperthermia 1990;6:421–430.
14. Losev E. Mathematical simulation of thermoregulation in local hyperthermia. Biophysics 1993;38:843–847.
15. Zaerr J, Roemer RB, Hynynen K. Computer-controlled dynamic phantom for ultrasound hyperthermia studies. IEEE Trans Biomed Eng 1990;37:1115–1118.
16. Chen C, Xu LX. Tissue temperature oscillations in an isolated pig kidney during surface heating. Ann Biomed Eng 2002;30:1162–1171.
17. Chen C, Xu L. Theoretical and experimental studies of local tissue temperature oscillation under hyperthermic conditions using preserved pig kidney. In: Proceedings of the ASME; 2000; International Mechanical Engineering Conference and Exposition, Orlando, FL, 2000;83–88.
18. Chen C, Xu LX. A vascular model for heat transfer in an isolated pig kidney during water bath heating. ASME J Heat Transfer 2003;125:936–943.
19. Levick J. An Introduction to Cardiovascular Physiology. London: Arnold, 2000.
20. Silva MRE, Antonio A. Release of bradykinin and the mechanism of production of a thermie edima (45°C) in the rat's paw. Medicina Experimentalis 1960;3:371–382.
21. Johnson P. Local regulatory mechanisms in the microcirculation. Introductory remarks. Fed Proc 1975;34:2005.
22. Moncada S, Palmer M, Higgs E. Nitric oxide: Physiology, pathophysiology, and pharmacology. Pharmacol Rev 1991;43:109–142.
23. Farrell D, Bishop V. Permissive role for nitric oxide in active thermoregulatory vasodilation in rabbit ear. Am J Physiol 1995;269:H1613–618.
24. Hall D, Buettner G, Matthes R, Gisolfi C. Hyperthermia stimulates nitric oxide formation: Electron paramagnetic resonance detection of NO-heme in blood. J Appl Physiol 1994;77:548–553.
25. Cosby K, Partovi KS, Crawford JH, Patel RP, Reiter CD, Martyr S, et al. Nitrite reduction to nitric oxide by deoxyhemoglobin vasodilates the human circulation. Nat Med 2003;9:1498–1505.
26. Stamler J. Hemoglobin and nitric oxide. New Engl J Med 2003;349:402–405.
27. Kniffki K, Mense S, Schmidt R. Muscle receptors with fine afferent fibers which may evoke circulatory reflexes. Circulation Res 1981;48:25–31.
28. Rowell L, O'Leary D, Kellogg D. Integration of cardiovascular control systems in dynamic exercise. In Section 12, Exercise: Regulation and Integration of Multiple Systems. In: Handbook of Physiology. New York: Oxford University Press, 1996.
29. Rowell L. Human Cardiovascular Control. New York: Oxford Press, 1993.
30. Lincoln J, Ralevic V, Burnstock G. Neurohumoral substances and the endothelium. In: Rubanyi GM, ed. Cardiovascular significance of endotherlium-derived vasoactive factors. Mount Kisco, NY: Futura Publishing Company, Inc., 1991.
31. Berne RM, Levy MN. Physiology. St. Louis, MI: Mosby, Inc., 1998.
32. Daanen H, Ducharme M. Axon reflexes in human cold exposed fingers. Eur J App Physiol 2000;81:240–244.
33. Chen C, Roemer RB. Modeling of transient tissue temperatures and biotransport of vasodilators during localized heating. In: 2003 International Mechanical Engineering Conference and Exposition; Washington DC, 2003.
34. Middleman S. Transport Phenomena in the Cardiovascular System. New York: Wiley-Interscience, 1972.

35. Welling PG. Pharmacokinetics. Washington, DC: American Chemical Society, 1997.
36. Rubanyi GM. Cardiovascular Significance of Endothelium-Derived Vasoactive Factors. Mount Kisco, NY: Futura Publishing Company, Inc., 1991.
37. Moros E. Experimental evaluation of two simple thermal models using hyperthermia in muscle *in vivo*. Int J Hyperthermia 1993;9:581–598.
38. Pennes H. Analysis of tissue and arterial blood temperatures in the resting human forearm. Appl Physiol 1948;1:93–122.
39. Ignarro L. Biological actions and properties of endothelium-derived nitric oxide formed and released from artery and vein. Circulation Res 1989;65:1–21.
40. Yang F, Troncy E, Francceur M, Vinet B, Vinary P, Czaika G, et al. Effects of reducing reagents and temperature on conversion of nitrite and nitrate to nitric oxide and detection of NO by chemiluminescence. Clin Chem 1997;43:657–662.
41. Sakai S, Takeoka S, Yokohama H, Seino S, Nishide H, Tsuchida E. Purification of concentrated hemoglobin using organic solvent and heat treatment. Protein Expression Purification 1993;4:563–569.
42. Tharp HS, Roemer RB. Optimal power depostion with finite-sized, planar hyperthermia applicator arrays. IEEE Trans Biomed Eng 1992;39:569–579.
43. Marcus ML, Bischof CJ, Heistad DD. Comparison of microsphere and xenon-133 clearance method in measuring skeletal muscle and cerebral blood flow. Circ Res 1981;48:748–761.
44. Kapin MA, Ferguson JL. Hemodynamic and regional circulatory alterations in dog during anaphylacTIc challenge. Am J Physiol 1985;249:G221–G227.
45. McDannold N. MRI Evaluation of thermal ablation of tumors with focused ultrasound. J Magn Reson Imag 1998;8:91–100.
46. Clavo B, Robaina F, Catala L, Valcarcel B, Morera J, Carames M, et al. Increased locoregional blood flow in brain tumors after cervical spinal cord stimulation. J Neurosurg 2003;98:1263–1270.
47. Koh T, Taniguchi H, Yamagishi H. Oxygen-15 positron-emission tomography for predicting selective delivery of a chemotherapeutic agent to hepatic cancers during angiotensin II-induced hypertension. Cancer Chemother Pharmacol 2003;51:349–358.
48. El-Farra NH, Christofides PD, Liao JC. Computational modeling of nitric oxide transport and consumption in blood vessels. In: The 41st IEEE Conference on Decision and Control; Las Vegas, Nevada, USA, December 2002.
49. Buerk DG. Can we model nitric oxide biotransport? A survey of mathematical models for a simple diatomic molecule with surprisingly complex biological activities. Ann Rev Biomed Eng 2001;3:109–143.